ingegneria sismica
International Journal of Earthquake Engineering
Anno XLIII - Num. 2 - 2026

Coupling mechanism of particle flow and mass transfer in fluidized bed reactor under multi-scale modeling

Xiaojiao Song[1,*] *and Yonghong Guo*[1]

[1] Department of Energy and Engineering, Shanxi Institute of Energy, Jinzhong, Shanxi, 030600, China

SUMMARY: *The movement rule of particles inside the fluidized bed reactor is a complex heat and mass transmission process that includes many phases and components. For the purpose of probing into the properties of granule flow and the heat transfer action among phases inside fluidized bed reaction devices, The academic circle's persons have carried out very many research works. In this article, on the basis of the mathematical model of dense gas-solid two-phase multiscale flow-reaction, the fluidization reaction is considered by us under the supposed conditions that influence factors include particle mass, momentum, temperature, energy and so on, we have put forward the related control equations, and we have chosen the Syamlal - O'Brien drag model for depicting the fluid drag force which acts on the particles. The doing of this is to carry out a numerical simulation work of the two-phase flow motion of two-component particles inside a gas-solid two-phase system.The experiment results showed that after we carry out the two-dimensional simulation of the gas-solid two-phase and two-component particle flow in the fluidized bed reactor, the distribution of particles in the Syamlal-O'Brien model is comparatively even on the whole bed. Furthermore, the particle density in the vicinity of the wall was about the value 4.291E+9. When we carry out examination of the particle Nusselt number at different time points, as the flow process goes forward, the whole particle Nusselt number is approximately limited within the scope of 0 to 0.7. This shows that the heat transfer capability within the fluidized-bed reactor is more uniform. In addition, researchers have found that the volumetric mass-transfer coefficients of gas and solid phases which are in the fluidized bed increase when initial gas velocity becomes larger, and decrease when the mass fraction of solid particles becomes higher.*

KEYWORDS: *multiscale flow-reaction; Syamlal-O'Brien tracer model; two-component particles*

1 Introduction

Fluidized bed reactor is a device commonly used for chemical reactions, heat transfer and mass transfer [1].The transfer work is completed through using the dynamic flowing state of the granule material layer. This method provides the advantages of fast reaction speeds and increased heat and mass transfer effectivenesses [2, 3]. This mechanism mainly includes the flowing characteristics of the fluidized bed, the motion rule of the granular material, and the heat and mass transmission which takes place in the whole process of the reaction [4]. In a fluidized bed reactor, the bed material is dynamically fluidized by hydrodynamic action [5]. Within the bed, the particulate material is dispersed in the gas stream and flows in an irregular

*songxiaojiao0930@163.com
https://doi.org/10.65102/is2026588
Published: 30 April, 2026

motion, creating a liquid-like flow pattern [6, 7]. This flow pattern is favorable for the reaction process because it increases the contact area of the reacting materials and improves the reaction rate [8].

In the fluidized bed reactor, the movement manner of granular materials also has very important significance for the reaction process [9]. Due to the collision and friction effects between the particulate materials, different modes of motion are generated, such as rolling, sliding, and collision [10, 11].The movement modes and velocities of the materials have very obvious influences on both the reaction and the transmission processes. Inside the fluidized bed reaction device, the heat and mass transfer processes which happen in the reaction time are also very important mechanisms [12]. The transference of heat and mass occurs as the consequence of the interaction between the granular material inside the bed and the gas current [13]. This transfer can effectively transfer heat and mass from the reacting material to the inside of the bed and increase the reaction rate and transfer efficiency [14, 15].Through using the combined action of the fluidized bed's flow characteristics, the motion rules of the granular material, and the heat and mass transmission that take place in the reaction process, the fluidized bed reactor can obtain the advantages of fast reaction, high-efficiency transmission, and stable working condition. This therefore makes it become a very excellent chemical reaction device [16-18]. For this target, this research puts emphasis on the fluidization reaction of two-component particles. This work carries out a three-dimensional numerical simulation on the flow and mass-transfer processes which exist inside the gas-solid two-phase system. We have established an Euler-Euler two-component particle fluidization model, this model is on the basis of the Syamlal-O'Brien tracer model. This model already makes the gas-solid multiphase flow and heat and mass transfer become one whole, and it also contains a particle mass-transfer submodel. The model then gives out results that are about flow features, heat transmission, and particle mass transfer of two different kinds of particles inside the fluidized bed. Numerical simulations of the flow characteristics, mass transfer characteristics, and coupling mechanisms of two different particles were performed, aiming to provide a reference for future research.

2 Method

2.1 Subjects of study

The experiments were carried out in a self-built fluidized bed which is made by transparent acrylic. For the purpose of conveniently observing the characteristics of the aggregate bodies that exist inside the fluidized bed, a piece of fluidized bed which possesses a sheet shape was utilized by us. The simplified structure diagram of this device arrangement is shown in Fig. 1. The fluidizing gas used in the test was air compressed by an air compressor and the two-component solid particles were silica gel and quartz sand particles. The air is compressed by the compressor device. After that, the compressed air passes through the buffer tank, and then passes through the flow meter, before it enters the base part of the fluidized bed. When the gas goes upward through the fluidized bed, it carries the material to the upper place through the lifting tube. In the course of this movement that takes place inside the fluidized bed, the particles do form aggregated masses. The mixing degree of the particles can be ascertained through collecting the material from the sampling position of the bed.Numerical simulation was carried out using commercial software ANSYS FLUENT 19.0. The height of the experimental setup is 2500m, which is divided into three zones: dense phase zone (0~500mm), transition zone (500~600m) and dilute phase zone (600~2500m).The inside diameters of the dense-phase zone and the rare-phase zone are 120 millimeters and 150

millimeters separately. The particle entering place is situated at a distance of 400 millimeters from the height of the bed, and the second air inlet is placed 600 millimeters from the bottom of the bed. In the physical model of this simulation, we put forward the postulate that particles do not have combustion process take place inside the cyclone separator. For cutting down the calculation work load, the User-Defined Function (UDF) is utilized by us. This UDF is employed to carry out the function of the two-component particles' outer circulation system, which thus acts to hold a constant amount of bed material inside the furnace. By means of an analysis on grid independence, it has been confirmed that a grid quantity of approximately 1.31 × 106 can meet the requirements of the Courant number and the ratio of the smallest time-steps. At the same time, this number of grid can guarantee the calculation precision.

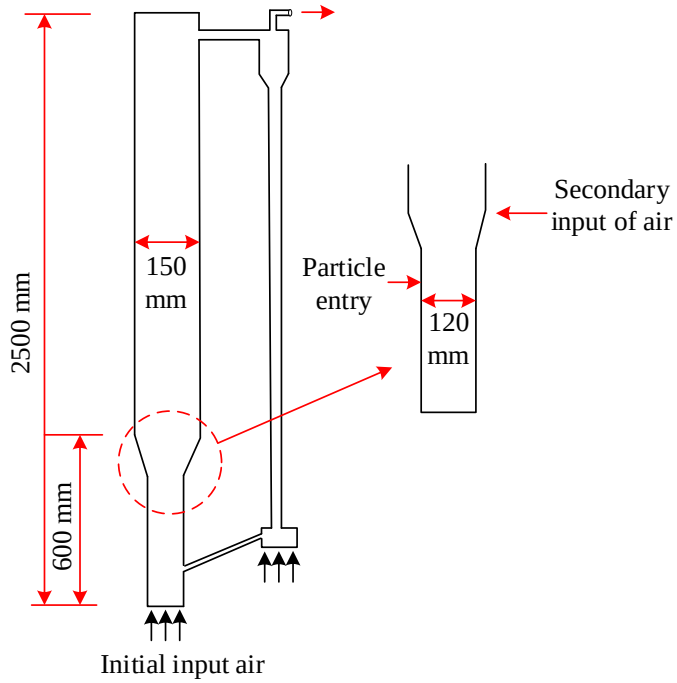

Figure 1: Simplified diagram of the experimental device

2.2 Control equations

2.2.1 Mass conservation equations

In this research work, a multiphase flow, together with the EMMS drag model inside a riser tube, is utilized to carry out simulations of the mixed multi-component gas-solid flow. The continuity equation, together with the momentum and energy conservation equations, is utilized, by which a clear separation is made for the gas and solid phases. In the two - composition particle model, the change in mass that is brought by chemical reactions has been considered. The equations which govern are given in below:

$$\frac{\partial}{\partial t}\left(\varepsilon_g \rho_g\right)+\nabla\cdot\left(\varepsilon_g \rho_g u_g\right)=S_{gs} \tag{1}$$

$$\frac{\partial}{\partial t}\left(\varepsilon_s \rho_s\right)+\nabla\cdot\left(\varepsilon_s \rho_s u_s\right)=S_{sg} \tag{2}$$

where S_{gs} and S_{sg} denote the source terms for the mass change between the gas-solid phases induced by chemical reactions, respectively:

$$S_{gs}=\sum_{i=1}^{N_g}S_{gs,i}\ S_{sg}=\sum_{i=1}^{N_s}S_{sg,i} \tag{3}$$

where $S_{gs,i}$ and $S_{sg,i}$ denote the mass increment per unit of time per unit of volume of the ith component in the gas and particle phases, respectively, and N_g and N_s denote the number of components in the gas and particle phases.

For particles consisting of a multi-component mixture, assuming an ideal gas, the density is determined by the ideal gas equation of state:

$$\frac{1}{\rho_g}=\frac{RT_g}{p}\sum\frac{X_{g,i}}{M_{g,i}} \tag{4}$$

where R is the universal gas constant, $R=8.314\text{J/(mol}\cdot\text{K)}$. $X_{g,i}$ and $M_{g,i}$ represent the mass fraction and molar mass of component i, respectively.

2.2.2 Equation of conservation of momentum

$$\begin{aligned}&\frac{\partial}{\partial t}\left(\varepsilon_g\rho_g u_g\right)+\nabla\cdot\left(\varepsilon_g\rho_g u_g u_g\right)=-\varepsilon_g\nabla p+\varepsilon_g\nabla\cdot\tau_g\\&+\varepsilon_g\rho_g g-\beta\left(u_g-u_s\right)+S_{gs}u_g\end{aligned} \tag{5}$$

$$\begin{aligned}&\frac{\partial}{\partial t}\left(\varepsilon_s\rho_s u_s\right)+\nabla\cdot\left(\varepsilon_s\rho_s u_s u_s\right)=-\varepsilon\nabla p-\nabla p_s\\&+\varepsilon_s\nabla\cdot\tau_s+\varepsilon_s\rho_s g+\beta\left(u_g-u_s\right)+S_{sg}u_s\end{aligned} \tag{6}$$

where β denotes the gas-solid interphase traction coefficient. In the coarse grid computing experiment of a fluidization bed reaction device, the effect of medium-scale structure is neglected. Therefore, inside the calculation grid, a multi-scale gas-solid interphase pull model which takes into account the influence of mesoscale structure is needed.

2.2.3 Particle-fitting temperature equations

$$\begin{aligned}&\frac{3}{2}\left[\frac{\partial}{\partial t}\left(\varepsilon_s\rho_s\theta\right)+\nabla\cdot\left(\varepsilon_s\rho_s\theta\right)u_s\right]\\&=\left(-\nabla p_s I+\tau_s\right):\nabla u_s+\nabla\cdot\left(k_s\nabla\theta\right)+\phi_s-\gamma_s+D_{gs}\end{aligned} \tag{7}$$

where k_s denotes the particle-phase heat transfer coefficient, in formula (7), the last three items separately represent the pulsation energy changes that come from momentum transmission, the consumption coefficient that comes from non-elastic collision between particle and particle, and the mutual actions between the pulsation speed of gas and the pulsation speed of particles.

2.2.4 Component mass conservation equations

$$\begin{aligned}&\frac{\partial}{\partial t}\left(\rho_g \varepsilon_g X_{g,i}\right)+\nabla\cdot\left(\rho_g \varepsilon_g u_g X_{g,i}\right)\\&=\nabla\cdot\left[\varepsilon_g\left(\rho_g D_{g,i}+\frac{\mu_{gt}}{Sc_t}\right)\nabla\cdot X_{g,i}\right]+S_{g,i}\end{aligned} \tag{8}$$

$$\begin{aligned}&\frac{\partial}{\partial t}\left(\rho_s \varepsilon_s X_{s,i}\right)+\nabla\cdot\left(\rho_s \varepsilon_s u_s X_{s,i}\right)\\&=\nabla\cdot\left[\varepsilon_s\left(\rho_s D_{s,i}+\frac{\mu_{st}}{Sc_t}\right)\nabla\cdot X_{s,i}\right]+S_{s,i}\end{aligned} \tag{9}$$

where $D_{g,i}$ and $D_{s,i}$ denote the diffusion coefficients of the gas-phase and particle-phase components i and Sc_t is the Schmidt number.

2.2.5 Energy conservation equation

In the research that this paper puts forward, we make the assumption that the influence of radiative heat transfer is got rid of consideration. Under this hypothesis, the energy conservation equation which is between the gas phase and the particle phase may be written out as follows:

$$\begin{aligned}&\frac{\partial}{\partial t}\left(\rho_g \varepsilon_g c_{pg} T_g\right)+\nabla\cdot\left(\varepsilon_g \rho_g u_g c_{pg} T_g\right)=\nabla\left[\varepsilon_g\left(\lambda_g+c_{pg}\frac{\mu_{gt}}{\mathrm{Pr}_t}\right)\nabla T_g\right]\\&+\frac{6}{d_s}\varepsilon_s h_{gs}\left(T_s-T_g\right)+\sum S_{g,i}c_{pg,i}T_g\end{aligned} \tag{10}$$

$$\begin{aligned}&\frac{\partial}{\partial t}\left(\varepsilon_s \rho_s c_{ps} T_s\right)+\nabla\cdot\left(\varepsilon_s \rho_s u_s c_{ps} T_s\right)=\nabla\left[\varepsilon_s\left(\lambda_s+c_{ps}\frac{\mu_{st}}{\mathrm{Pr}_t}\right)\nabla T_s\right]\\&+\frac{6}{d_s}\varepsilon_s h_{gs}\left(T_g-T_s\right)+\sum S_{s,i}c_{ps,i}T_s\end{aligned} \tag{11}$$

where λ_g and λ_s denote the thermal conductivity of the gas and particle phases, respectively, Pr_t is the Prandtl number, and c_{pg} and c_{ps} denote the gas and particle phase Constant-pressure specific heat capacity, which is obtained from a polynomial regression equation with temperature as a variable. The h_{gs} this thing represents the coefficient that is about heat transmission between the gas phase and the solid phase. This coefficient may be obtained from an equation which has relation to the Nusselt number of the particle phase.

$$h_{gs}=\frac{\lambda_g \varepsilon_g}{d_s}Nu_s \tag{12}$$

where d_s is the single particle diameter and Nu_s is the particle phase Nussel number,

which can be expressed as:

$$\begin{aligned} Nu_s = &\left(7-10\varepsilon_g+5\varepsilon_g^2\right)\left(1+0.7\,\mathrm{Re}_s^{0.2}\,\mathrm{Pr}_t^{1/3}\right) \\ &+\left(1.33-2.4\varepsilon_g+1.2\varepsilon_g^2\right)\mathrm{Re}_s^{0.7}\,\mathrm{Pr}_t^{1/3} \end{aligned} \tag{13}$$

In the circulating fluidized bed reactor, the presence of particle agglomerates makes the bed show a multi-scale flow structure, which leads to the heat transfer between gas-solid phases to show a certain non-uniformity accordingly, so it is necessary to carry out a multi-scale solution for the heat transfer coefficients between gas-solid phases, in order to better reproduce the heat transfer law between gas-solid phases.

2.3 Towing force model

In the gas-solid two-phase flow which is inside a fluidized bed reactor, the movement of particles is affected by the fluid. The forces which are exerted by the gas flow upon the particles can be divided into drag force and traction force. When the speed of the particles surpasses that of the liquid, this force is shown to be resistance, and when the liquid speed is bigger than the particle speed, it is displayed as pulling force.In the present research paper, the Syamlal-O'Brien drag model is utilized by us to depict the drag force that is exerted by the fluid upon two-component particles. This model may obtain good prediction results when we carry out numerical simulation experiments on the gas-solid two-phase flow that contains class D particles.

When $\varepsilon_g > 0.8$, Ergun's equation is used to obtain:

$$F_{yj} = \frac{3}{4} C_d d \rho \frac{\varepsilon_y \rho_y}{\varepsilon_y^2} \left|u_g - v_g\right|^2 \left(u_g - v_g\right) \tag{14}$$

When $\varepsilon_g \le 0.8$, using Wen&Yu equation yields:

$$F_{yj} = \left[150\frac{\left(1-\varepsilon_g\right)}{\varepsilon_g}\frac{\mu_g}{d_p^2} + 1.75\frac{\rho_g}{d_p}\frac{\left|u_g - v_g\right|}{\varepsilon_g}\right]\left(u_g - v_g\right)V_p \tag{15}$$

where: $\dot{C}_d$ - effective traction coefficient.

ε_g -gas density $\left(\mathrm{kg}\cdot\mathrm{m}^{-3}\right)$.

V_p -particle volume $\left(\mathrm{m}^3\right)$.

d_p -particle diameter $\left(\mathrm{m}\right)$.

u_g -gas velocity $\left(\mathrm{m}\cdot\mathrm{s}^{-1}\right)$.

v_g -particle velocity $\left(\mathrm{m}\cdot\mathrm{s}^{-1}\right)$.

μ_g -gas shear viscosity $\left(\mathrm{Pa}\cdot\mathrm{s}\right)$.

$$C_d' = C_d \varepsilon_g^{-n} \tag{16}$$

where: n -correction factor for bed void fraction.

C_d -Trailing coefficient of single particles.

$$C_d = \begin{cases} \dfrac{24}{\mathrm{Re}_p}\left(1+0.15\,\mathrm{Re}_p^{0.678}\right)\cdots\cdots\left(\mathrm{Re}_p<1000\right) \\ 0.44\cdots\cdots\cdots\cdots\cdots\cdots\left(\mathrm{Re}_p\geq 1000\right) \end{cases} \tag{17}$$

The particle Reynolds number is calculated as:

$$\mathrm{Re}_p = \frac{\varepsilon_g \rho_g \left|u_g - v_g\right| d_p}{\mu_g} \tag{18}$$

2.4 Two-component particle mass transfer modeling

People widely hold the view that the fluidized bed has a very large heat storage capacity. Therefore, when we carry out the examination of the mass transfer phenomenon of two-component particles that exist inside a fluidized bed, this process can be regarded by us as an isothermal one.In this research paper, the mass transmission that happens between the gas phase and solid phase of two-component particles is controlled by the mass transmission mechanism. The adsorbing speed of reacting gases is connected with the mass passing coefficient, the total surface area of active granules, and the difference in the density of reacting gases on the surface of active granules that are inside the emulsified phase. The concrete formula expressions are given below:

$$\frac{dN_m}{d_t} = S_p K_g \left(C_{m,pe} - C_{m,ps}\right) \tag{19}$$

where: $\dfrac{dN_m}{d_t}$ - adsorption rate of the reacting gas;

K_g - mass transfer coefficient (m/s);

S_p -Total area of active particles (m^2);

$C_{m,pe}$ -concentration of reaction gas around the particles in the emulsified phase (g/m3);

$C_{m,ps}$ - the density of gas (which is measured by gram per cubic meter) on the surface of the particulates that lie inside the emulsified phase.

The formulation which is for the coefficient of mass transfer k_g is shown below:

$$k_g = Sh \times D_m / D_p \tag{20}$$

where: Sh (Sherwood number) - dimensionless parameter closely related to the mass transfer between gas and solid;

D_m -diffusion rate of reaction gas (m^2/s).

After many years of experiments by previous generations to obtain the expression of Sh (Sherwood number) there are a variety of expressions, respectively, applied to different fluidized bed mass transfer process research, the most basic expression method is built upon the analysis of invariance analysis and the analysis of boundary layer theory. The above

analyses come from the Reynolds number (Re) and the Schmidt number (Sc), which are built to give the following result:

$$Sh = k + b + \mathrm{Re}^{c} \times \mathrm{Sc}^{d} \tag{21}$$

where the values of k, b, c and d are determined on a case-by-case basis. The expression can be regarded as two parts, which are convective mass transfer in the first term and diffusive mass transfer in the second term. In this paper, the empirical formula of Sh, which meets the working condition of the mass transfer study in this paper, is selected according to the needs of the study, i.e., the formula of Sh, which is proposed on the basis of considering the phenomenon of particle aggregation:

$$Sh = 2 \times \varepsilon_g + 0.69 \times \varepsilon_g \times \left[(\mathrm{Re}/\varepsilon_g)^{a} \times \mathrm{Sc}^{b} \right] \tag{22}$$

It is applied to a subsequent study in the mass transfer section of this paper to analyze the mass transfer characteristics of a two-component particulate system.

3 Results

3.1 Analog parameter settings

In this paper, two-component particles are simulated, for which the initial bed material static height is 50 mm. According to the analysis of the experimental bed material properties, the stacking density of quartz sand (coarse) particles is 0.2, and the stacking density of silica gel (fine) particles is 0.4, and the maximal particles stacking limit is 0.65. For the purpose of making the comparison between the results and the experimental discoveries more effective, therefore, we put forward the hypothesis that in the simulation of two components, the diameter of the small silica gel granules is 0.3 millimeters, and the diameter of the big silica gel granules is 1 millimeter.For the purpose of making the comparison with experiment results become more effective, we put forward a hypothesis that in the two-component simulation work, the grain diameter of fine silica gel is 0.3 mm, therefore the grain diameter of coarse quartz sand is 1 mm. The composition of this gas is air, it is specifically 21% oxygen and 79% nitrogen. The entrance is arranged as a speed entrance, and the exit is established as a pressure exit. A non-slip boundary condition is utilized between the gas phase and the wall, and a partial-slip boundary condition is applied between the solid phase and the wall.

Table 1: Simulation parameter settings

Parameter setting	Value	Parameter setting	Value
Silica gel (SG) particle size /mm	0.3	SG density/$(\mathrm{kg \cdot m^{-3}})$	1000
Quartz sand (QS)Particle size /mm	1	QS density/$(\mathrm{kg \cdot m^{-3}})$	2000
Specific heat of grain/$(\mathrm{J \cdot (kg \cdot K)^{-1}})$	1000	Mixed particle thermal conductivity/ $(\mathrm{W \cdot (m \cdot K)^{-1}})$	0.5
Molecular weight/$(\mathrm{kg \cdot mol^{-1}})$	10	Particle collision recovery coefficient	0.8
Excess air coefficient	1.0	Initial bed height /mm	200
Primary air temperature /K	500	Initial temperature /K	1123
Secondary air temperature /K	300	Proportion of primary wind	0.6
Return material temperature /K	500	Proportion of primary wind	0.4

Outlet pressure /Pa	-50	Time step	0.001

3.2 Two-dimensional simulation of gas-solid two-phase flow in a fluidized bed reactor

3.2.1 Fluidization process simulation

Figure 2 has described that in the fluidized bed reactor, at different time points, the distribution of the volume fraction of two-component particles exists. When the simulation begins by the way of putting gas into the fluidized bed reactor, bubbles begin to be generated at the lower part of the bed. When these bubbles go upward, they slowly become bigger. By the effect of the gas trailing force, the particles of two components carry out upward movement, the jet in the upward extension of the process, the central aggregation area of the particles of the role of gravity began to fall, while the bubble rupture. When the particles drop down and are again subjected to the action of the gas, the bed expands again, and then the bed transitions to a steady state.In the fluidized bed reaction device, the distribution of granule density has the character of non-uniform. Two phases, which are the dilute phase and the dense phase, have obvious differences. The extra gas which is inside the bed constitutes bubbles that rapidly pass through the bed. This gas-solid fluidization system exists in an obvious aggregated fluidization condition. When t equals to 1.6 second, the particle's concentration has an uneven distribution around the center place, and four obvious low-concentration spots have come out. The density of the particles in that time point was approximately 4.295E+9.

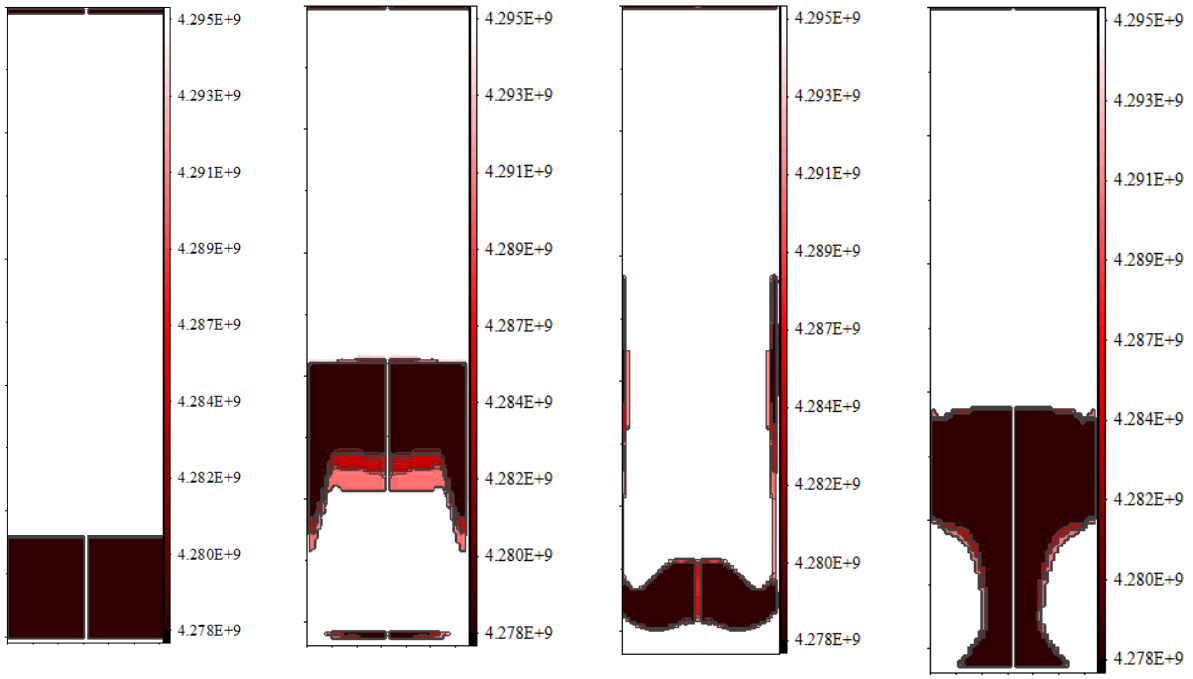

(a)t=0s (b)t=0.2s (c)t=0.4s (d)t=0.8s

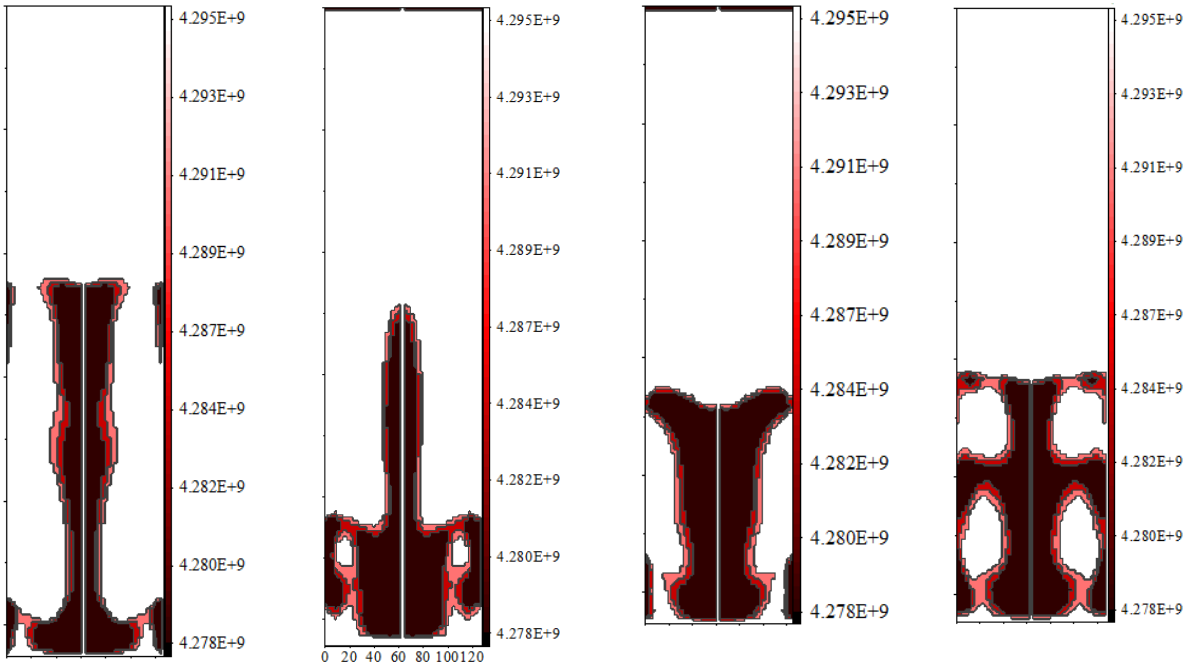

(e)t=1s (f)t=1.2s (g)t=1.4s (h)t=1.6s

Figure 2: The distribution of particle volume fractions at different times in the fluidized bed

3.2.2 Effect of initial bed height on fluidization characteristics

This paper also has carried out a detailed exploration about the fluidization characteristics of two-component particles that are inside a fluidized bed. We have carried out the investigations when the starting bed heights are 50 mm, 70 mm, and 90 mm. Therefore, the pressure drop curves have been obtained, which is shown in Figure 3. From this figure, we can clearly see that between the initial height of the bed and the pressure drop of the bed, there exists a direct connection. Therefore, the larger the initial height of the bed, the higher the pressure drop value of the bed. Nevertheless, the gas speed at which the pressure drop gets stable still keeps unchangeable, which is measured as 0.1 m/s.When the initial height of the bed is more great, the static pressure which is inside the bed becomes more high, hence the pressure drop is more significant after the gas enters it. When the gas velocity reaches 0.1 m per second, the gravitation force that acts on the particles is equal to the resistance force that is exerted by the gas. When the heights of the bed layer are 50 millimeters, 70 millimeters, and 90 millimeters, the corresponding drag force values are 380 Pa, 543 Pa, and 694 Pa each separately.After the bed layer attains the critical fluidization state, the gas velocity has the continuous rising. But, the pressure falling inside the bed layer keeps unchanged. This illustrates that the critical fluidization speed for two-component particles is only decided by the dimension and properties of the particles, and is not influenced by the starting height of the bed.

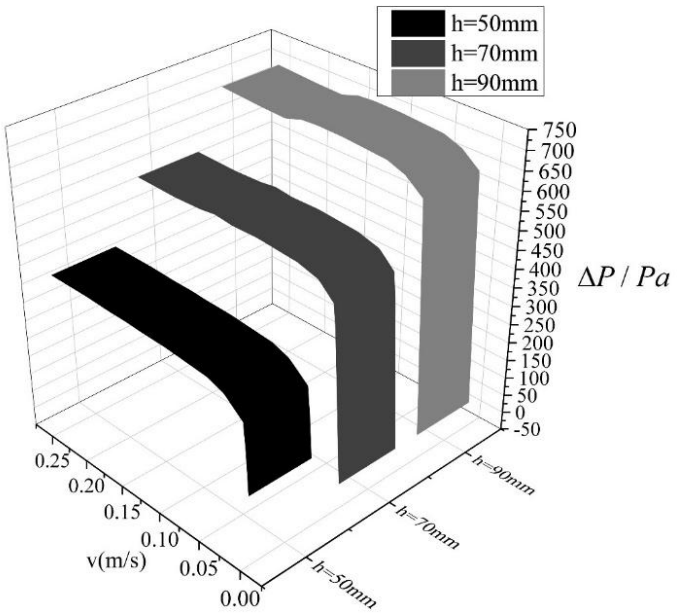

Figure 3: Pressure drop curves at different initial bed heights

3.2.3 Effect of particle size on fluidization characteristics

The Figure 4 gives the pressure drop curves which belong to silica gel and quartz sand. These materials are made up of particles that have two different diameters, and they are put into a fluidized bed reactor which has an initial bed height that is 50 mm. Along with the increment of particle diameter, the critical fluidization gas velocity presents an increasing trend, while the pressure drop exhibits a decreasing tendency. This situation happens, therefore, because when the particle's diameter becomes bigger, the particle's mass also increases. For the particle to keep staying in the suspended state, it must carry out counteraction against a comparatively larger gravitation force. Therefore, thus, the critical speed of fluidization gas for the bed layer becomes higher.When the starting mass of the particles increases, the particle size will let the particle packing density get lower, and the gap between the particles will become bigger. When gas with the same velocity go through these empty places, the resistant force becomes smaller, and the drop of pressure inside the fluidized-bed reactor also gets lower. In the figure, the fluidization curves of particle size d=0.5mm and d=1mm have a raised section where the pressure drop increases and then decreases. The fluidization curve of d=0.5mm suddenly decreases at the moment of v=0.25m/s, and the pressure drop continues to decrease from 387Pa to about 358Pa at last, while the fluidization curve of d=1mm decreases from 370Pa to 330Pa when v=0.43m/s. 330Pa was maintained. While the fluidization curve for particle size d=0.25mm is not. This is probably because the increase in particle size changes the particles from class A to class B, and the fluidization characteristics of the particles also change. The reason for the raised portion can be ascribed to the random character and absence of uniformity in the distribution of particles, and also the friction that exists between the particles. Before the pressure drop arrives at the weight of the bed in each unit area, the resistance which makes the whole bed expand can definitely have an increase. After the bed completes the full fluidization process, the distribution of particles turns relatively even, and the friction force among particles becomes smaller. At this time point, the pressure fall of the bed arrives at the level that corresponds to the ordinary fluidization condition.

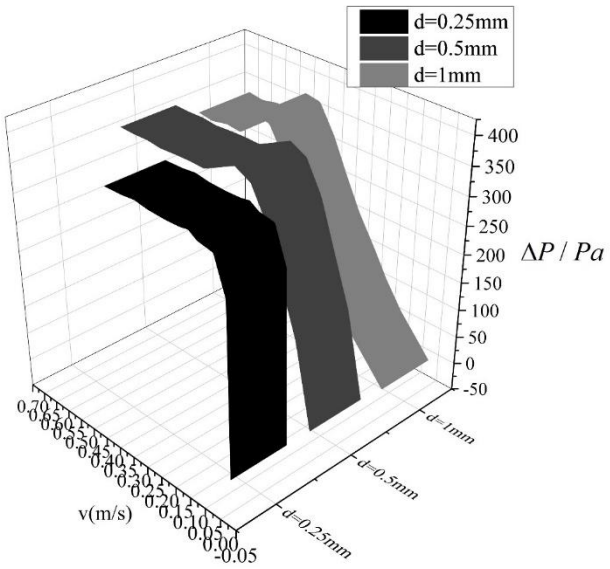

Figure 4: Pressure drop curves of particles of different diameters

3.3 Flow and mass transfer characterization of two-component particles in a fluidized bed

3.3.1 Nussel number distribution of two-component particles

Figure 5 has described the distributing situation of the particle Nusselt number under different bed height conditions. This diagram gives the distribution situation of the particle Nusselt number on different time points and bed height positions. When the bed height has the measurement of 50 mm, the particle Nusselt number at the beginning is low when the flow starts its occurrence. The peak numerical value of the particle Nusselt number can reach approximately 10.69. As the process proceeds, the water in the particle system evaporates, the particles are gradually fluidized, the Nussell number gradually increases, and the heat transfer capacity in the fluidized bed reactor increases. When the bed height was 90 mm, the particle Nussel number increased significantly, and the maximum value was about 11.86, indicating that the heat exchange capacity in the upper part of the bed was stronger. In addition, with the drying process, the particle Nussel number distribution gradually showed symmetrical distribution.

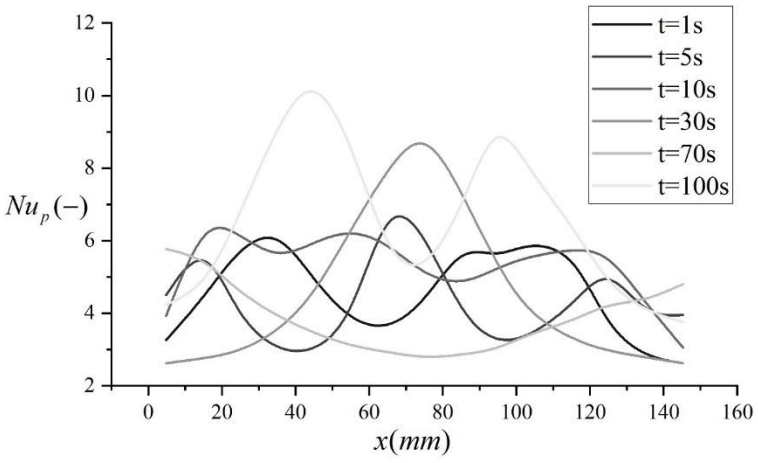

(a)h=50mm

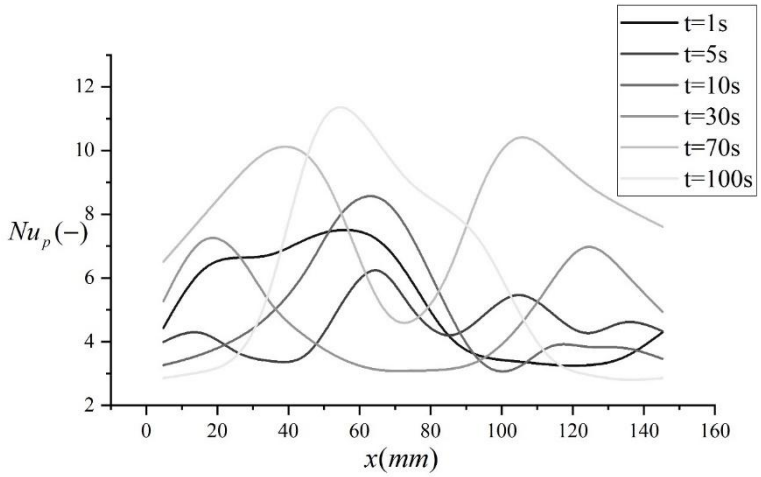

(b)h=90mm

Figure 5: The distribution of the particles of the sand in different bed height

3.3.2 Heat transfer capacity in fluidized bed reactors

Figure 6 has shown the change of the particle Nusselt number regarding the particle volume fraction on different time points. From this picture, we can see that when the particle volume fraction goes up, therefore, the heat-transfer ability is decreased, and the particle Nusselt number drops. Furthermore, along with the process going forward, the distribution scope of the particle Nusselt number has almost no change. Taking everything into consideration, it is gathered inside the scope from 0 to 0.7. Under the condition of same particle volume fraction, the distribution situation of particle Nusselt number becomes more concentrated. This hence indicates that the ability of heat transmitting which is inside the fluidized-bed reactor is more even.

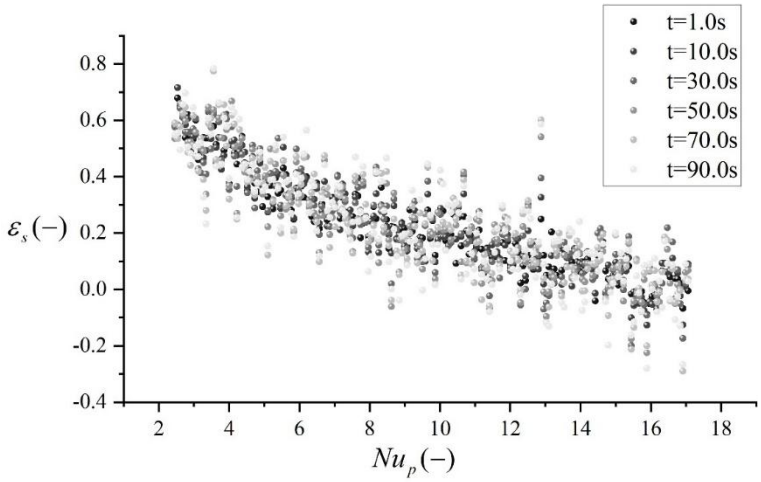

Figure 6: At different moments, the number of nuzz is the fraction of the particle

3.3.3 Distribution of heat flow in the form of heat transfer

Figure 7 has shown the distributing situation of each kind of heat transfer way at different time points and different bed height positions. According to what is shown in Figure 7 (a) and (b), when the bed height is 50 mm, in the starting stage of the drying process (t = 5 s and 10 s), the heat flux among particles by the heat conduction approach reaches maximum values of

0.107 and 0.088 separately, with the drying process, the particles of the temperature gradually converges to the same, the heat flux between the particles is gradually reduced. At the same time, along with the temperature of the granules inside the bed gradually becoming consistent, the difference in temperature between the granules continuously becomes smaller. Therefore, the heat current among the granules gradually gets close to 0 W.When the height of the bed reaches 90 millimeters, the distribution of heat flux among particles through heat conduction is in accordance with that in the middle of the bed, hence it displays no obvious difference. Figure 7(c) and 7(d) give out the distributions of heat flow between gas and particles, and also the distribution of heat flow among particles via heat conductance, when bed heights are 50 millimeters and 90 millimeters.In the Figure 7(a) and 7(b), the trend is opposite to the distribution situation of the heat flow between the particles. When the particles lie in a completely fluidized condition, the contact area between the gas and the solid becomes larger. As a consequence, the heat flow between the gas and the solid continuously increases in the drying process, attaining maximum values of 0.013 and 0.053 respectively.

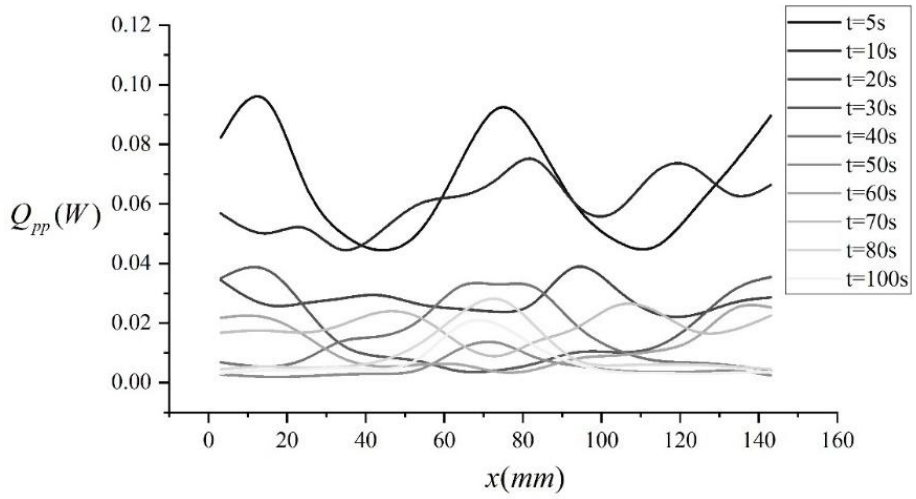

(a)h=50mm,Particle heat conduction flow rate

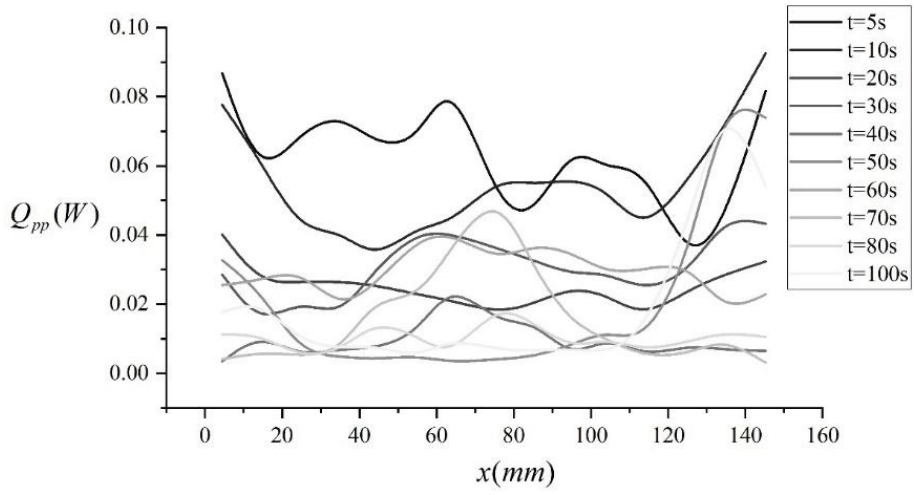

(b)h=90mm,Particle heat conduction flow rate

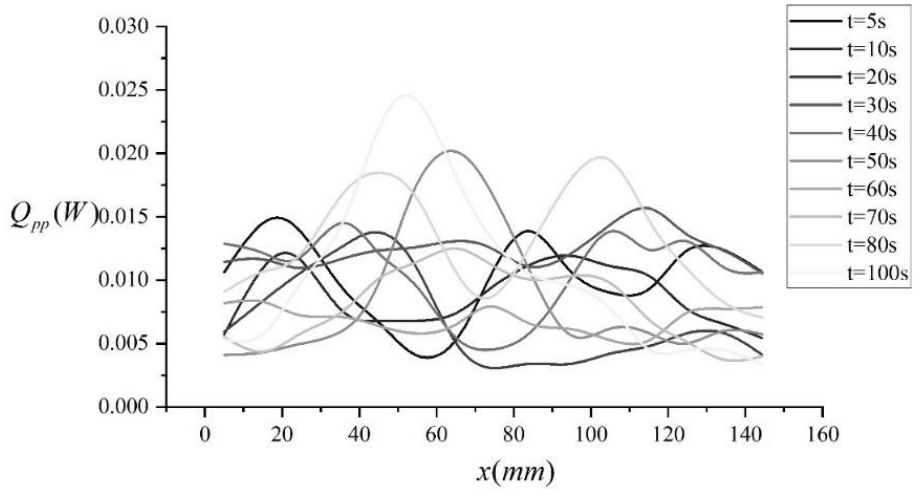

(c)h=50mm, Convective heat flow between gas and solid

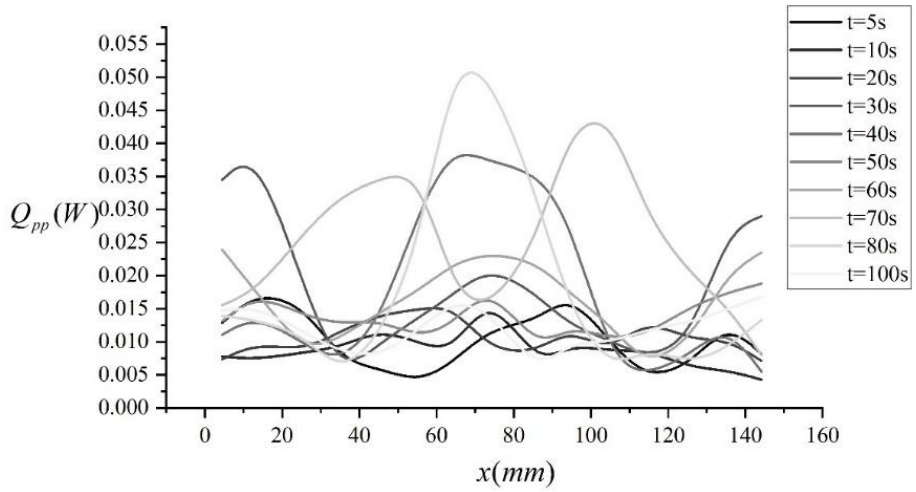

(d) h=90mm, Convective heat flow between gas and solid

Figure 7: Different times, different bed height, different heat exchange forms

4 Conclusion

In this paper, the assumed conditions are added to the governing equations in a two-component particle model. For the purpose of more accurately replicating the rule of gas-solid interphase heat transmission, factors including momentum, the proposed temperature of particles, conservation of component quality, conservation of energy, and other related elements are all taken into consideration. This action is taken for the calculation of gas-solid interphase heat transfer coefficients on many different scales.One coupling model for gas-solid two-phase systems has been established by us to carry out simulation works on the gas-solid two-phase flow which is inside the fluidized bed reactor. This model also had the aim to carry out examination of the correlation between the flow behavior of particles and the characteristics of mass transfer. By means of simulation and analysis, the mass fraction distribution of particles that have different particle sizes and densities at different heights within a two-component particle bed has been obtained. In the process of fluidization, people have discovered that the mass proportion of small-dimension particles in the bottom part of

the bed has a gradual decrease, while their mass proportion in the middle and upper parts of the bed has a gradual increase. By comparison, big-volume particles displayed the reverse trend. In addition, inside the experiment working range, it was observed that the volume mass transfer coefficients of the gas-solid two-phase two-component particle fluidized bed rose when the initial gas speed rose. Under this background, the increase of the gas initial velocity mainly caused an enlargement of the gas content and the phase-boundary region inside the fluidized bed. Along with the increment of the mass fraction that solid particles possess, the dimensionless number which represents the mass-transfer coefficient for the mass transfer that occurs between solid particles and air is in a gradual process of decline.

Funding

Research Project: "Study on Flow and Mass Transfer Characteristics of Multicomponent Particles in Fluidized Bed Reactors" Shanxi Institute of Energy Institutional-Level Scientific Research Fund Project, Project No. ZY-2023022

References

[1] Yates, J. G., & Lettieri, P. (2016). Fluidized-bed reactors: processes and operating conditions (Vol. 26, p. Springer). New York: Springer.

[2] Wu, K., Francia, V., & Coppens, M. O. (2020). Dynamic viscoplastic granular flows: A persistent challenge in gas-solid fluidization. Powder Technology, 365, 172-185.

[3] Blanco, A., & Chejne, F. (2016). Modeling and simulation of biomass fast pyrolysis in a fluidized bed reactor. Journal of analytical and applied pyrolysis, 118, 105-114.

[4] Michel, R., Kaknics, J., de Bilbao, E., & Poirier, J. (2016). The mechanism of agglomeration of the refractory materials in a fluidized-bed reactor. Ceramics International, 42(2), 2570-2581.

[5] Mellin, P., Kantarelis, E., & Yang, W. (2014). Computational fluid dynamics modeling of biomass fast pyrolysis in a fluidized bed reactor, using a comprehensive chemistry scheme. Fuel, 117, 704-715.

[6] Zbib, M. B., Dahl, M. M., Sahaym, U., Norton, M. G., Osborne, E. W., & Bahr, D. F. (2012). Characterization of granular silicon, powders, and agglomerates from a fluidized bed reactor. Journal of materials science, 47(6), 2583-2590.

[7] Izquierdo-Barrientos, M. A., Sobrino, C., Almendros-Ibáñez, J. A., Barreneche, C., Ellis, N., & Cabeza, L. F. (2016). Characterization of granular phase change materials for thermal energy storage applications in fluidized beds. Applied Energy, 181, 310-321.

[8] Zhang, H., Qiao, W., An, X., Ye, X., & Chen, J. (2022). CFD-DEM study on fluidization characteristics of gas-solid fluidized bed reactor containing ternary mixture. Powder Technology, 401, 117354.

[9] Liu, G. (2018). Application of the two-fluid model with kinetic theory of granular flow in liquid–solid fluidized beds. Granularity in Materials Science, 2.

[10] Chladek, J., Jayarathna, C. K., Moldestad, B. M., & Tokheim, L. A. (2018). Fluidized bed classification of particles of different size and density. Chemical Engineering Science, 177, 151-162.

[11] Suksomboon, R., Junsiri, C., Tangjitjaroenkit, S., El-Moselhy, M. M., & Padungthon, S. (2019). Mathematical models of a fluidized bed bioreactor using granular activated carbon (FBBR-GAC) for wastewater treatment. Engineering and Applied Science Research, 46(3), 183-191.

[12] Zhu, L. T., Liu, Y. X., & Luo, Z. H. (2019). An enhanced correlation for gas-particle heat and mass transfer in packed and fluidized bed reactors. Chemical Engineering Journal, 374, 531-544.

[13] Li, Z., Janssen, T. C. E., Buist, K. A., Deen, N. G., van Sint Annaland, M., & Kuipers, J. A. M. (2017). Experimental and simulation study of heat transfer in fluidized beds with heat production. Chemical engineering journal, 317, 242-257.

[14] Abdelmotalib, H. M., Youssef, M. A., Hassan, A. A., Youn, S. B., & Im, I. T. (2015). Heat transfer process in gas–solid fluidized bed combustors: A review. International Journal of Heat and Mass Transfer, 89, 567-575.

[15] Oppong, F. (2018). Recent studies of heat transfer mechanisms in a fluidized bed. R&D Journal, 34, 72-82.

[16] Menéndez, M., Herguido, J., Bérard, A., & Patience, G. S. (2019). Experimental methods in chemical engineering: Reactors—fluidized beds. The Canadian Journal of Chemical Engineering, 97(9), 2383-2394.

[17] Hamers, H. P., Romano, M. C., Spallina, V., Chiesa, P., Gallucci, F., & van Sint Annaland, M. (2014). Comparison on process efficiency for CLC of syngas operated in packed bed and fluidized bed reactors. International journal of greenhouse Gas Control, 28, 65-78.

[18] Abdelmotalib, H. M., & Im, I. T. (2017). Three dimensional modeling of heat transfer and bed flow in a conical fluidized bed reactor. International Journal of Heat and Mass Transfer, 106, 1335-1344.